nature microbiology

LETTERS

https://doi.org/10.1038/s41564-019-0455-0

# Microfluidic-based transcriptomics reveal force-independent bacterial rheosensing

Joseph E. Sanfilippo[1,6], Alexander Lorestani[1,6], Matthias D. Koch[1,2], Benjamin P. Bratton[1,2], Albert Siryaporn[1,3,4], Howard A. Stone[5] and Zemer Gitai[1*]

**Multiple cell types sense fluid flow as an environmental cue. Flow can exert shear force (or stress) on cells, and the prevailing model is that biological flow sensing involves the measurement of shear force[1,2]. Here, we provide evidence for force-independent flow sensing in the bacterium *Pseudomonas aeruginosa*. A microfluidic-based transcriptomic approach enabled us to discover an operon of *P. aeruginosa* that is rapidly and robustly upregulated in response to flow. Using a single-cell reporter of this operon, which we name the flow-regulated operon (*fro*), we establish that *P. aeruginosa* dynamically tunes gene expression to flow intensity through a process we call rheosensing (as *rheo-* is Greek for flow). We further show that rheosensing occurs in multicellular biofilms, involves signalling through the alternative sigma factor FroR, and does not require known surface sensors. To directly test whether rheosensing measures force, we independently altered the two parameters that contribute to shear stress: shear rate and solution viscosity. Surprisingly, we discovered that rheosensing is sensitive to shear rate but not viscosity, indicating that rheosensing is a kinematic (force-independent) form of mechanosensing. Thus, our findings challenge the dominant belief that biological mechanosensing requires the measurement of forces.**

Mechanical features shape how organisms interact with their environment such that there are often selective benefits for cells to sense them. While eukaryotic mechanosensing has been studied extensively[1,2], bacterial mechanosensing has been appreciated only recently[3,4]. Most studies on mechanosensing have focused on surface sensing, but fluid flow is also an important mechanical cue. Flow is present in many environments where bacteria thrive, such as hosts and associated medical devices. Recent reports have shown that bacteria sense flow to modulate gene expression and signalling[5,6]. In enterohemorrhagic *Escherichia coli*, expression of the locus of enterocyte effacement virulence factors is induced by flow and host association[5], and in *Pseudomonas aeruginosa*, cyclic-di-guanosine monophosphate levels are induced by flow and surface attachment[6]. In theory, cells could sense flow by sensing changes in shear rate (the kinematic component of flow) or shear stress (the force-related component of flow). In the best-characterized example of biological flow sensing, mammalian cells use the force-sensitive von Willebrand factor to recruit platelets in response to fluid flow[1]. By analogy, other cellular systems that sense flow, including the bacterial responses described above, have been interpreted to be triggered by shear force[5,6]. However, the conclusion that cells sense flow by measuring shear force has not been directly tested in these systems.

To enable a biophysical characterization of bacterial flow sensing, we focused on the bacterium *P. aeruginosa* and began with a global assessment of how it changes its transcriptome in response to flow. Specifically, we developed an experimental system that subjects cells to flow in microfluidic channels and monitors global gene expression through RNA sequencing (RNA-Seq; Fig. 1a). We discovered a large number of changes in gene expression after four hours of exposure to flow (Supplementary Table 1). To focus on the potential direct targets of flow, we repeated our analysis after only 20 min of flow exposure (Fig. 1b and Supplementary Table 2). A previously unnamed four-gene operon was the most highly induced operon at this early time point (Fig. 1c). While all four genes in this operon were expressed at relatively low levels (all in the bottom 50% of the genome by expression) before flow exposure, they exhibited strong induction after 20 min of flow exposure (approximately ~13-fold; Fig. 1c). Thus, we focused our efforts on this operon as a model for the broader flow response and named its four genes *froA-D* (for flow responsive operon).

To probe the *P. aeruginosa* flow response with single-cell resolution, we engineered a two-colour fluorescent reporter strain that reports on *fro* expression with yellow fluorescent protein (YFP) and uses constitutively expressed mCherry for normalization (Supplementary Fig. 1). In straight microfluidic channels (Fig. 1d), YFP fluorescence increased approximately sixfold in flow, while mCherry fluorescence remained constant (Fig. 1e and Supplementary Fig. 2). These results validate our transcriptional profiling data and show that individual *P. aeruginosa* cells induce *fro* expression in response to flow. We call this form of bacterial environmental sensing rheosensing, as the prefix *rheo-* is Greek for flow.

*P. aeruginosa* often exists in biofilms in nature—especially in environments with flow[7]. Therefore, we examined rheosensing in the context of multicellular communities, focusing on flow-induced biofilm streamers that we generated in microchannels featuring a series of 90° bends (Fig. 1f). Biofilms are aggregates of bacteria held together by an extracellular matrix. Biofilm streamers occur under specific conditions of flow in which the biofilm remains attached to the surface at a focal point while a long tendril of cells and matrix extends into the centre of the channel[7]. We detected *fro* expression throughout the cells in biofilm streamers, including in cells significantly removed from the channel surface (Fig. 1g). Therefore, *P. aeruginosa* cells within a multicellular community are capable of rheosensing.

[1]Department of Molecular Biology, Princeton University, Princeton, NJ, USA. [2]Lewis-Sigler Institute for Integrative Genomics, Princeton University, Princeton, NJ, USA. [3]Department of Physics and Astronomy, University of California, Irvine, Irvine, CA, USA. [4]Department of Molecular Biology and Biochemistry, University of California, Irvine, Irvine, CA, USA. [5]Department of Mechanical and Aerospace Engineering, Princeton University, Princeton, NJ, USA. [6]These authors contributed equally: Joseph E. Sanfilippo, Alexander Lorestani. *e-mail: zgitai@princeton.edu

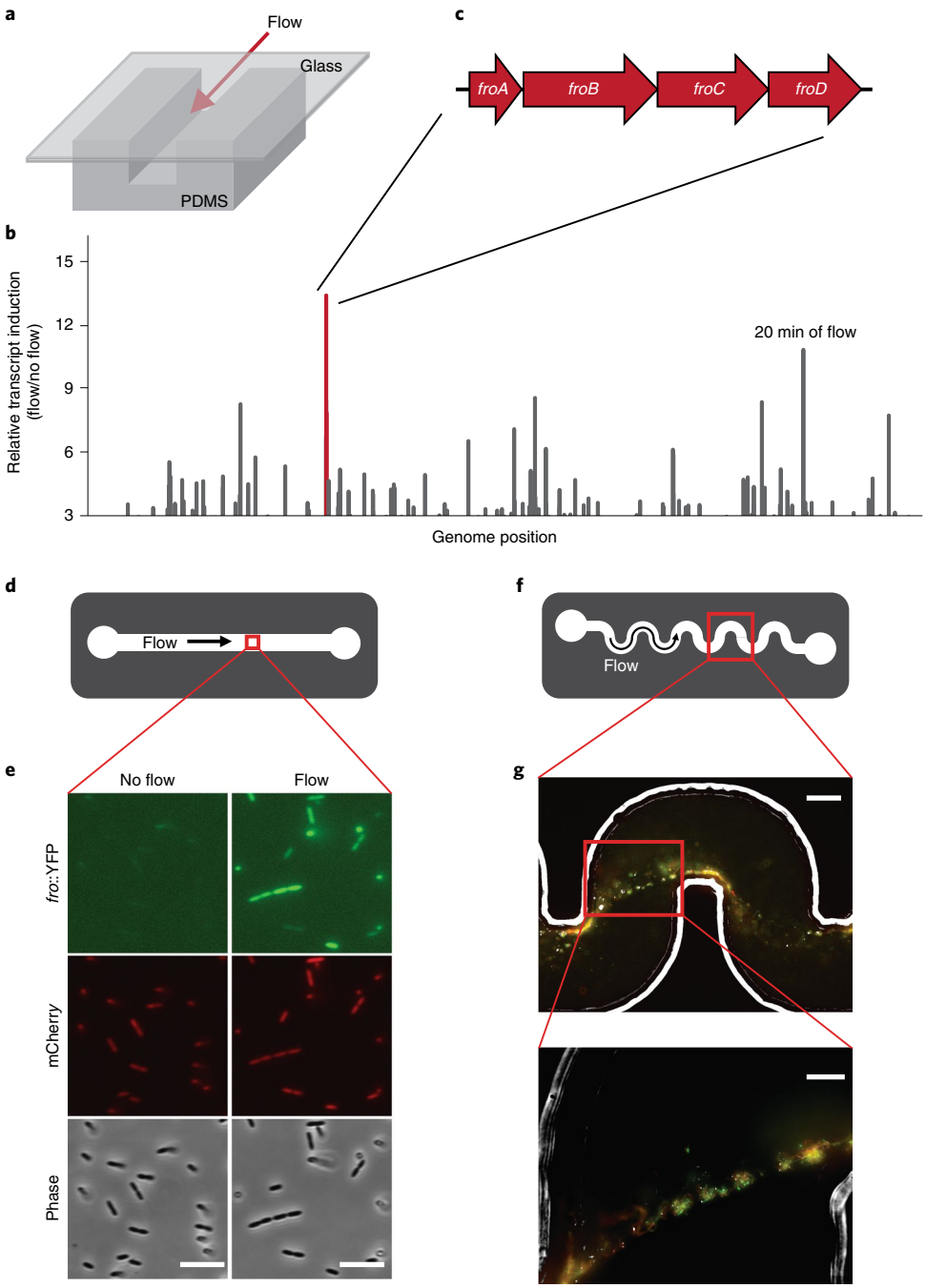


**Fig. 1 | Flow triggers the induction of gene expression in *P. aeruginosa*.** **a**, Schematic of the microfluidic device used throughout this study. Channels are custom-fabricated from polydimethylsiloxane (PDMS) and glass. **b**, Fold-change in the transcript abundance of *P. aeruginosa* cells subjected to flow for 20 min relative to flow-naive cells. Line heights linearly correspond to fold-changes and are plotted as a function of the genomic location on the *P. aeruginosa* chromosome. Only genes induced at least threefold are represented. The raw data used to generate this graph are presented in Supplementary Table 2. The red line corresponds to the *fro* operon. **c**, The *fro* operon. **d**, Schematic depicting the view from above the microchannel used in **e**. These channels were 50 μm tall × 500 μm wide. **e**, Fluorescence and phase images of the *fro* reporter strain in straight microfluidic channels before and after 4 h of 10 μl min$^{-1}$ flow. Images are representative of three independent experiments. Scale bars, 5 μm. **f**, Schematic of the microchannel used in **g**. These channels were 90 μm tall × 100 μm wide. **g**, Top, merged image of phase, YFP and mCherry from a single optical plane of a representative streamer biofilm projecting off the wall of a microchannel. Scale bar, 50 μm. Bottom, magnified view of the cells not directly in contact with the channel surface. Scale bar, 20 μm. Images are representative of three independent experiments. Streamers were cultured in 2 μl min$^{-1}$ flow for 20 h.

The single-cell response of the *fro* reporter enabled us to quantitatively characterize the response of *P. aeruginosa* to flow. The flow experienced by bacteria on a surface depends on the bulk flow rate and channel geometry. To represent flow intensity in a geometry-independent manner, we report the shear rate, which is the rate at which adjacent layers of fluid pass one another. We explored the dynamic range of rheosensing by examining *fro* expression after cells were subjected to a range of shear rates for 2 h. *fro* induction did not occur at low shear rates (8 s$^{-1}$), increased in response to intermediate shear rates (40–400 s$^{-1}$), and plateaued at high shear

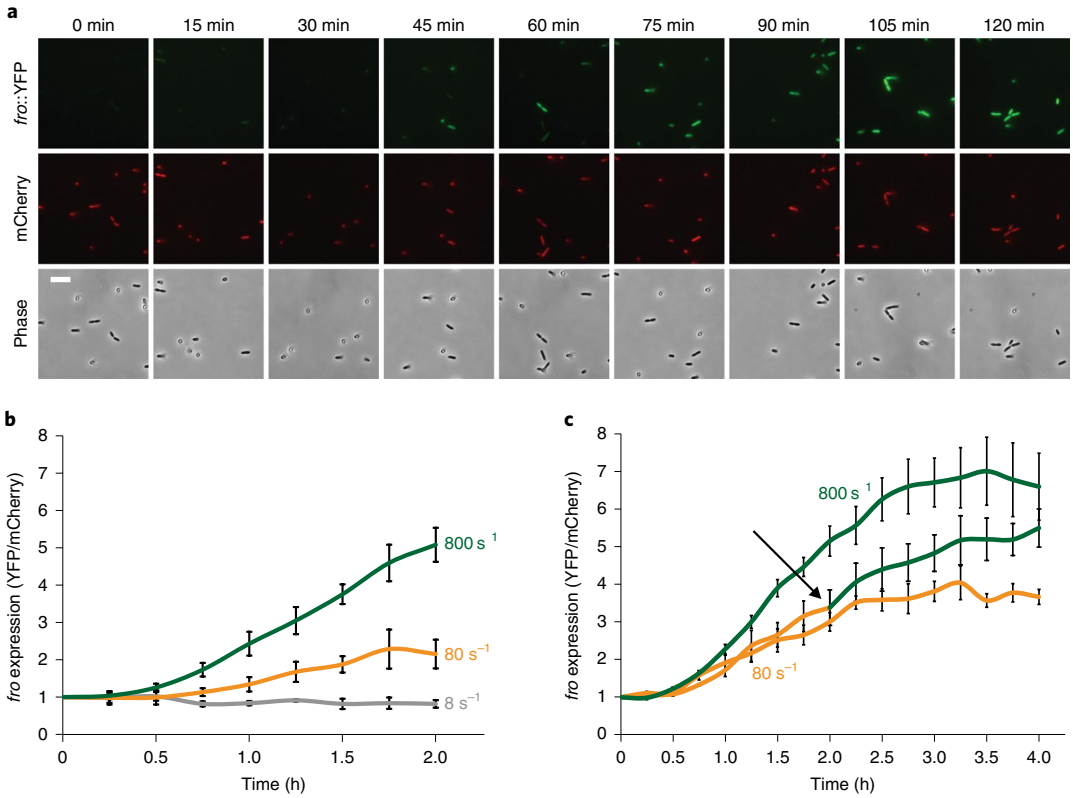


**Fig. 2 | The shear rate rapidly and dynamically tunes rheosensing. a**, Images of cells exposed to flow at a wall shear rate of 800 $s^{-1}$ over 120 min. Top, *fro* reporter (YFP) channel. Middle, mCherry normalization control channel. Bottom, phase contrast channel. Images are representative of three independent experiments. Scale bar, 5 μm. **b**, *fro* expression over 2 h in the presence of 8 (grey line), 80 (yellow line), and 800 $s^{-1}$ (green line) shear rates. At 2 h, the 8 $s^{-1}$ and 80 $s^{-1}$ samples are statistically different from each other with $P = 0.03$. At 2 h, the 80 $s^{-1}$ and 800 $s^{-1}$ samples are statistically different from each other with $P = 0.008$. **c**, *fro* expression over 4 h of time in the presence of 80 $s^{-1}$ (yellow line), 800 $s^{-1}$ (green line) or an upshift from 80–800 $s^{-1}$ (yellow/green line). The black arrow depicts the 2 h time point during which the shear rate was increased from 80–800 $s^{-1}$ for the upshifted sample. At 4 h, the upshifted sample resulted in *fro* expression that was statistically different from the 80 $s^{-1}$ sample with $P = 0.03$. Statistical significance in **b** and **c** was calculated by two-sided *t*-test. Error bars show the s.e.m. of three independent replicates. Each replicate represents quantification from 50 cells. *fro* expression at $t_0$ was set to 1. The channels used for these experiments were 50 μm tall × 500 μm wide.

rates (>400 $s^{-1}$) (Supplementary Fig. 3). To formally test the hypothesis that *fro* induction is modulated by shear rate, we also altered the channel height while maintaining a constant flow rate (the equation in Supplementary Fig. 3 shows how channel dimensions relate shear rate and flow rate). Increasing the channel height tenfold significantly reduced *fro* induction (Supplementary Fig. 3). Together, our results show that *fro* induction is not binary and is tuned by shear rate. These data also establish that rheosensing is tuned to a physiologically relevant range of shear rates[8], such as those found in average-sized human veins (~100 $s^{-1}$) and arteries (~650 $s^{-1}$).

Shear rate could modulate the kinetics of *fro* induction or the maximum amplitude of *fro* induction. We thus temporally characterized rheosensing by measuring *fro* expression over time at a range of shear rates. *fro* induction began at approximately 45 min (Fig. 2a,b), which was consistent with the maturation time of the YFP reporter used in this experiment[9]. Intermediate and high shear rates induced *fro* expression with different kinetics, as higher shear rates led to more rapid *fro* induction (Fig. 2b and Supplementary Fig. 4). The slope of the *fro* induction curve shows that induction saturates (Fig. 2c and Supplementary Fig. 4), indicating that rheosensing also sets the maximum amplitude of induction. Consistent with the ability of rheosensing to respond to changes in shear rate, cells saturated by exposure to intermediate flow for 2 h experienced additional *fro* induction when shifted to higher flow (Fig. 2c). Therefore, we conclude that this type of rheosensing is a tightly controlled sensory modality that fine-tunes the kinetics and amplitude of gene regulation in response to flow.

As rheosensing leads to changes in gene expression, we aimed to discover the regulatory factors that control rheosensitive signalling. We focused on two previously uncharacterized genes directly upstream from the *fro* operon that are predicted to encode an alternative sigma factor and anti-sigma factor[10]. Deletion of the putative sigma factor eliminated *fro* induction in flow, while deletion of the putative anti-sigma factor increased *fro* expression in flow-naive cells (Fig. 3a and Supplementary Fig. 5). Based on these results, we named the gene encoding the sigma factor '*fro* regulator' (*froR*) and the gene encoding the anti-sigma factor '*fro* inhibitor' (*froI*). Overexpression of *froR* increased *fro* expression, while overexpression of *froI* eliminated *fro* induction (Fig. 3a and Supplementary Fig. 5). Together, our results provide evidence for a model where the anti-sigma factor FroI antagonizes the alternative sigma factor FroR to control induction of the *fro* operon in flow.

Both flow and surfaces exert mechanical forces on cells such that they could use common sensors. To test whether rheosensing is related to previously proposed forms of bacterial mechanosensation, we asked whether the genes required for surface sensing are required for *fro* induction. Retraction of the type IV pilus controls surface sensing in *P. aeruginosa*[6,11–14] and *Caulobacter crescentus*[15]. However, retraction of the type IV pilus does not control rheosensing, as *fro* induction is maintained in Δ*pilA* (lacking

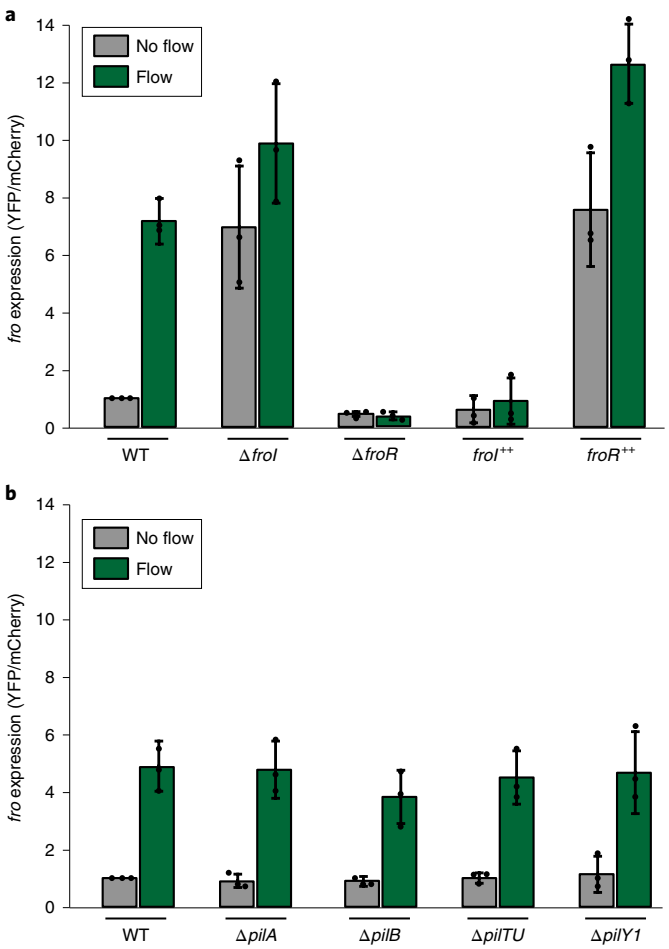


**Fig. 3 | *fro* induction requires the sigma factor FroR and anti-sigma factor FrpI, but not known surface sensors. a**, *fro* expression levels in wild-type (WT) cells, Δ*frpI* mutant cells, Δ*froR* mutant cells, *frpI*$^{++}$ overexpressing cells and *froR*$^{++}$ overexpressing cells subjected either to no flow (grey bars) or 2 h of flow at a shear rate of 800 $s^{-1}$ (green bars). Under the no flow condition, WT expression was significantly different from Δ*frpI* ($P = 0.04$), Δ*froR* ($P = 0.008$) and *froR*$^{++}$ expression ($P = 0.02$), but statistically indistinguishable from *frpI*$^{++}$ expression ($P = 0.18$). Under the flow condition, WT expression was significantly different from Δ*froR* ($P = 0.002$), *frpI*$^{++}$ ($P = 0.0005$) and *froR*$^{++}$ expression ($P = 0.01$), but statistically indistinguishable from Δ*frpI* expression ($P = 0.14$). **b**, *fro* expression levels in WT cells, Δ*pilA* mutant cells, Δ*pilB* mutant cells, Δ*pilTU* mutant cells and Δ*pilY1* mutant cells subjected either to no flow (grey bars) or 2 h of flow at a shear rate of 800 $s^{-1}$ (green bars). Error bars show the s.d. of three independent replicates and points indicate values for each replicate. Under the flow condition, WT expression was statistically indistinguishable from Δ*pilA* ($P = 0.88$), Δ*pilB* ($P = 0.28$), Δ*pilTU* ($P = 0.76$) and Δ*pilY1* ($P = 0.95$) expression. In **a** and **b**, statistical significance was calculated by two-sided *t*-test. Values were normalized to the WT under the no flow condition, which was set to 1 for each replicate. The channels used for these experiments were 50 μm tall × 500 μm wide.

the pilus fibre), Δ*pilB* (lacking pilus extension) and Δ*pilTU* (lacking pilus retraction) mutant backgrounds (Fig. 3b and Supplementary Fig. 6). Similarly, whereas PilY1 is required for surface-activated virulence in *P. aeruginosa*[16], *fro* induction was still observed in a Δ*pilY1* mutant (Fig. 3b and Supplementary Fig. 6). We also tested mutants lacking flagella, since the flagellum has been implicated in surface sensing in other bacteria[17,18]. As is the case for type IV pili and PilY1, the flagellum is not required for *fro* induction, as *fro* induction was also observed in a Δ*fliC* mutant (Supplementary Fig. 7)[19]. We note that none of the mutations tested dramatically disrupted adhesion (Supplementary Figs. 5–7) and that *fro* induction was normalized on a single-cell basis (Supplementary Fig. 1 describes our quantification pipeline). Additional support for the independence of rheosensing from surface sensors came from analysis of our transcriptional profiling, which revealed no statistical overlap between *P. aeruginosa* genes induced by flow and those induced by surface association (Supplementary Fig. 8)[16].

To directly test whether surface association alone is sufficient to induce *fro* expression, we fabricated microfluidic channels with flow-exposed and flow-shielded regions (Fig. 4a). While the bacteria in the flow-shielded regions did not experience flow, they remained surface associated for the duration of the experiment. Cells in flow-exposed regions of the channel induced *fro* expression approximately ninefold, while cells in flow-shielded regions did not (Fig. 4b and Supplementary Fig. 9). As an additional test of whether surface association affects rheosensing, we used the chemical 3-mercaptopropyl trimethoxysilane (MPTMS), which increases adhesion between *P. aeruginosa* and the channel surface[20]. MPTMS treatment did not affect *fro* induction (Supplementary Fig. 10), suggesting that cells perform rheosensing independent of how they attach to the surface. Together, our data indicate that *fro* induction is independent of known surface sensors, is not triggered by surface association itself, and is not affected by enhanced surface adhesion.

The independence of rheosensing from previously proposed forms of bacterial mechanosensing called into question the prevailing model that bacteria sense flow by measuring force. Fluid flow in a microfluidic channel has a kinematic aspect (shear rate, in units of time$^{-1}$) and a force-related aspect (shear stress, in units of force/area)[21]. These two aspects are linked by the viscosity of the solution, as shear stress is the product of shear rate and viscosity (Fig. 4c)[21]. The finding that *fro* expression is tuned by flow intensity thus enabled us to use changes in viscosity to directly test whether *P. aeruginosa* responds to shear rate or shear force. To modulate viscosity, we used solutions with varying concentrations of the viscous agent Ficoll. These Ficoll solutions act as Newtonian fluids[22] and we directly quantified their viscosity at the scale of a bacterial cell using optical tweezers and micrometre-scale beads (Fig. 4d). Microscopic measurements of the viscosity of Ficoll solutions increased exponentially with concentration: 5% Ficoll increased the viscosity twofold, 10% Ficoll increased the viscosity fivefold, and 15% Ficoll increased the viscosity tenfold (Fig. 4d). If *fro* expression was triggered by shear force (or stress), we should have observed a linear relationship between viscosity and *fro* expression when the shear rate was held constant. To our surprise, we found that increasing the viscosity up to tenfold had no effect on *fro* expression at an intermediate shear rate (80 $s^{-1}$; Fig. 4e). To control for the possibility that Ficoll has deleterious effects on bacteria, we confirmed that Ficoll did not affect the full *fro* induction that occurs at a high shear rate (800 $s^{-1}$; Fig. 4f). Together, these experiments show that this form of rheosensing is a force-independent sensory modality.

The observation that *fro* induction is sensitive to shear rate but not shear force raises the question of whether rheosensing should be considered a form of mechanosensing. Traditionally, the field of mechanics encompasses the study of both motion and force. For example, kinematics is the subfield of mechanics that focuses on motion and deformation while ignoring forces, and the force-independent property of shear rate is considered a fundamental feature of fluid mechanics. Meanwhile, in biological contexts, the term mechanosensing has traditionally been restricted to the study of how cells sense force, potentially leading to premature conclusions about the nature of mechanosensing. The argument over whether kinematic rheosensing should be considered a type of mechanosensing or a distinct process is semantic, but its implications are significant. We suggest that it is more useful to consider rheosensing a

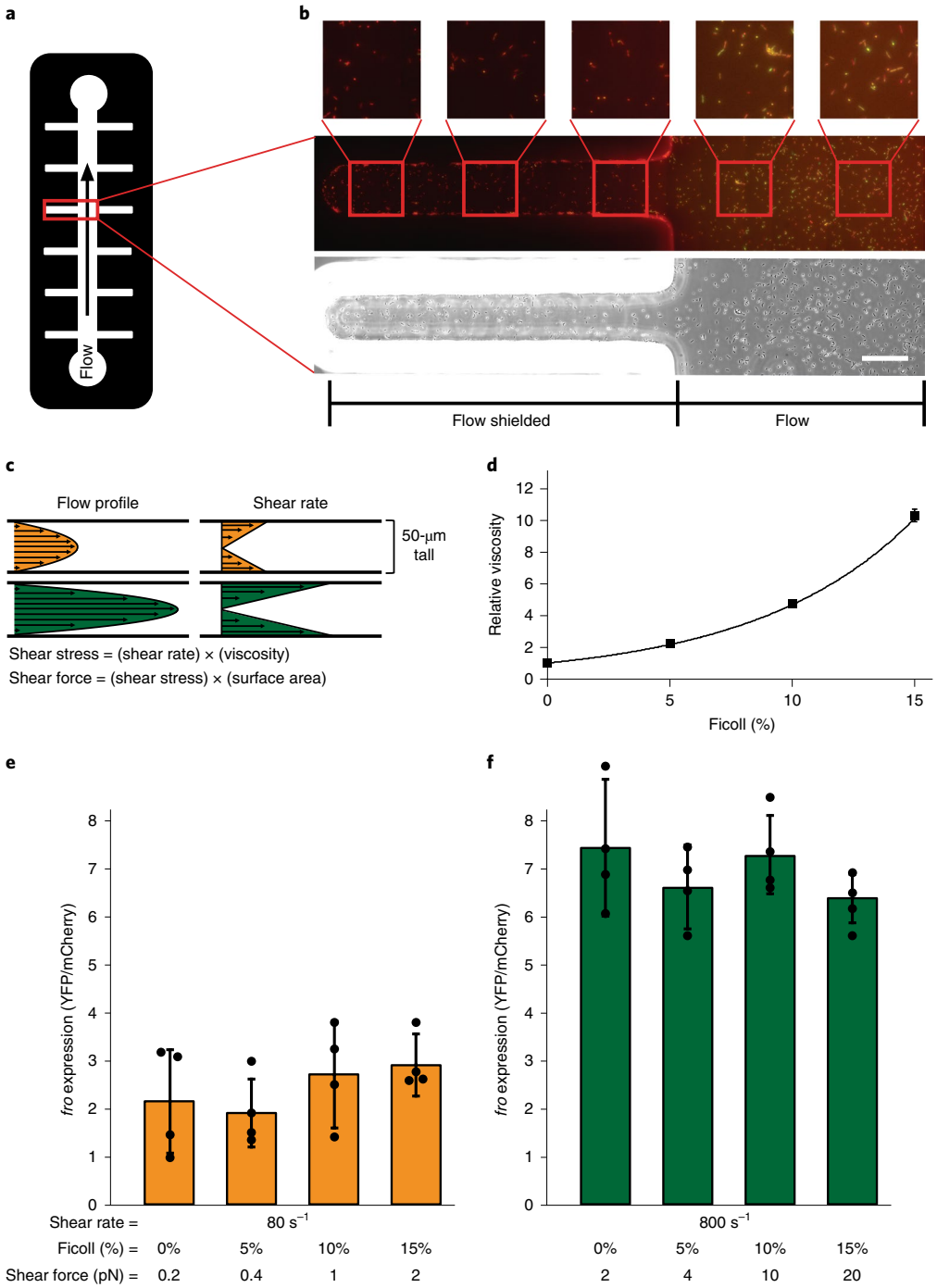


**Fig. 4 | Rheosensing is a force-independent sensory modality. a**, Schematic of the microchannel used in **b**. **b**, Merged YFP/mCherry images (top) and a phase image (bottom) of *fro* reporter cells in flow-exposed and flow-shielded regions of the channel after treatment at a shear rate of 800 $s^{-1}$ for 4 h. Scale bar, 50 μm. Images are representative of two independent replicates. **c**, Schematic showing how the flow profile corresponds to shear rate in a microfluidic device. The equations show that shear stress is the product of shear rate and fluid viscosity, and shear force is the product of shear stress and surface area. **d**, Microscopic viscosity of Ficoll solutions as measured with micrometre-scale beads and optical tweezers. Error bars show the s.d. of three independent replicates. **e**,**f**, Expression of the *fro* reporter in response to 2 h of flow at shear rates of 80 $s^{-1}$ (**e**) and 800 $s^{-1}$ (**f**) and the defined shear forces. Shear forces were calculated by multiplying shear stress by cell surface area, which was estimated at 2.5 $\mu m^2$. Error bars show the s.d. of four independent replicates, and points indicate values for each replicate. *fro* expression at 80 $s^{-1}$ was significantly different from *fro* expression at 800 $s^{-1}$ with treatments of 0% ($P = 0.003$), 5% ($P = 0.002$), 10% ($P = 0.002$) and 15% Ficoll ($P = 0.006$). *fro* expression at 80 $s^{-1}$ with no Ficoll was significantly indistinguishable from *fro* expression at 80 $s^{-1}$ with 5% ($P = 0.79$), 10% ($P = 0.67$) and 15% Ficoll ($P = 0.37$). *fro* expression at 800 $s^{-1}$ with no Ficoll was significantly indistinguishable from *fro* expression at 800 $s^{-1}$ with 5% ($P = 0.33$), 10% ($P = 0.66$) and 15% Ficoll ($P = 0.10$). Statistical significance in **e** and **f** was calculated by two-sided *t*-test. The *fro* expression of cells before flow treatment was set to 1. Channels used for these experiments were 50 μm tall × 500 μm wide.

form of mechanosensing as it provides proof-of-principle that cells can sense mechanical features of their environment such as flow without measuring force.

One potential benefit of force-independent rheosensing is that such a system robustly measures the speed of flow independent of other fluid properties such as viscosity. Thus, by sensing shear rate instead of shear force, *P. aeruginosa* could induce *fro* expression similarly across a wide range of different fluids, such as those found in freshwater streams, medical devices, the blood stream or lung sputum. Consistently, genomic studies indicate that the *froABCD* operon and gene encoding the sigma factor FroR are required for colonization of environments that have fluids that vary widely in viscosity, such as the lung[23] and gastrointestinal tract[24]. Furthermore, while the precise physiological role of rheosensing remains to be determined, genomic analysis of flow-induced genes identified a significant number of genes that are also induced during human infection (Supplementary Fig. 8)[25].

How might bacteria sense flow independent of force? Our finding that *fro* induction is modulated by shear rate suggests that the bacteria have a mechanism for measuring a rate-dependent biophysical process. Biological processes that are rate dependent but force independent include chemical transport and rotational diffusion. For example, flow has previously been shown to impact quorum sensing[26] and this effect is probably dependent on shear rate as higher flow would more rapidly wash away autoinducer. However, rheosensing is induced by flow rather than inhibited by it. Nevertheless, we tested the role of quorum sensing in rheosensing by assaying *fro* induction in a *lasR* mutant that eliminates canonical *P. aeruginosa* quorum sensing. We found that the loss of *lasR* had no effect on *fro* induction (Supplementary Fig. 11), suggesting that if rheosensing involves chemical transport it does so through a different system than quorum sensing that has not previously been shown to be flow sensitive.

Another possibility is that *P. aeruginosa* has a surface-exposed protein that directly senses shear rate. For example, a surface protein with asymmetrical domains would be predicted to rotate in a shear-rate-dependent manner, forming a molecular 'water wheel'. While understanding the molecular mechanism of shear rate sensing will require future studies, we know that rheosensing involves signalling through the extracytoplasmic function-family sigma factor FroR and the anti-sigma factor FroI. As neither *froR* nor *froI* RNA abundance is regulated by shear flow, post-translational regulation is probably involved in rheosensitive signalling. Extracytoplasmic function-family sigma factors and their corresponding anti-sigma factors have traditionally been implicated in sensing extracytoplasmic cues[27], such that FroR and FroI are well positioned to link the extracellular input of shear rate to the intracellular output of transcription.

Our discovery that cells can sense flow without sensing shear force suggests that there is value in re-evaluating the interpretation of biological responses to flow. Most responses to flow to date have not been thoroughly characterized at the biophysical level. However, a few well-understood examples in mammalian cells involve sensing shear force, such as platelet aggregation induced by the force-sensitive von Willebrand factor[1] or ion channel regulation by force-sensitive stereocilia in cochlear hair cells[2]. Based on analogy to these examples and the intuitive ability to understand how flow can impart a force (or stress), showing that a system is sensitive to flow has often been interpreted as evidence that the system responds to shear force[5,6]. Together, our results suggest the possibility of kinematic (force-independent) mechanosensing, which challenges the potentially premature conclusion that bacteria sense flow by measuring shear force. Future biophysical studies in both eukaryotes and bacteria will be required to test whether rheosensing is sensitive to shear force in other biological systems. It will be particularly interesting to determine whether the differences between bacterial and mammalian rheosensing reflect generalizable differences; for example, in the need for bacteria to respond to different fluids in contrast with the relatively uniform environments of most mammalian cell types.

## Methods

**Strains, plasmids and growth conditions.** The bacterial strains used in this study are described in Supplementary Table 3, the primers used are described in Supplementary Table 4 and the plasmids used are described in Supplementary Table 5.

*P. aeruginosa* was grown in liquid LB Miller (Difco) in a roller drum, and on LB Miller agar (1.5% Bacto Agar) at 37 °C. Antibiotics (Sigma–Aldrich) were used at the following concentrations: carbenicillin, 150 μg ml$^{-1}$ (liquid) and 300 μg ml$^{-1}$ (solid); gentamicin, 15 μg ml$^{-1}$ (liquid) and 30 μg ml$^{-1}$ (solid); tetracycline, 100 μg ml$^{-1}$ (liquid) and 200 μg ml$^{-1}$ solid; and irgasan, 25 μg ml$^{-1}$ solid.

*E. coli* was grown in liquid LB Miller (Difco) in a floor shaker, and on LB Miller agar (1.5% Bacto Agar) at 37 °C. Antibiotics (Sigma–Aldrich) were used at the following concentrations: carbenicillin, 50 μg ml$^{-1}$ (liquid) and 100 μg ml$^{-1}$ (solid); tetracycline, 7.5 μg ml$^{-1}$ (liquid) and 15 μg ml$^{-1}$ solid; and irgasan, 25 μg ml$^{-1}$ solid.

The *fro* reporter was generated using the lambda Red recombinase system[28]. The *fro* reporter construct was Gibson-assembled from three PCR products in the following series: (1) the 546 base pairs (bp) upstream from the target insertion site amplified from PA14 genomic DNA; (2) a 1,903-bp fragment containing a strong bacterial ribosome binding site, a YFP open reading frame (ORF) and an *aacC1* ORF flanked by flippase recombinase target sites amplified from pAS03; and (3) the 531 bp downstream from the target insertion site amplified from PA14 genomic DNA. Deletions in the *fro* reporter background were generated by the lambda Red recombinase system using the *aacC1* ORF between the flanking regions of the targeted gene of interest.

Constructs targeting the attTn7 phage attachment site were delivered by co-electroporation with pTNS2 (ref. [29]). Constructs targeting the *attB* phage attachment site were delivered by conjugation with an S17-1 strain harbouring a mini-CTX2 derivative[30].

**RNA-Seq library preparation and data analysis.** Total RNA was harvested from cells in fluidic devices by replacing medium with total lysis solution (10 mM Tris-HCl, 1 mM ethylenediamine tetraacetic acid, 0.5 mg ml$^{-1}$ lysozyme and 1% sodium dodecyl sulfate) and flowing through the device. Total lysis solution was incubated at room temperature for 2 min, then mixed with sodium citrate (pH 5.2) to 0.1 M. The resulting solution was mixed 1:1 with 0.1 M citrate-saturated phenol (pH 4.3), incubated at 64 °C for 6 min, and centrifuged for 10 min at 13,000*g* at 4 °C. The aqueous layer was mixed 1:1 with chloroform, transferred to phase lock tubes (Quanta Bio) and centrifuged for 10 min at 13,000*g* at 4 °C. The aqueous layer was precipitated by mixing 1:2 with a solution of 30:1 ethanol:3 M sodium acetate (pH 5.2), washing with 70% ethanol, and resuspending the resulting pelleting with water. Genomic DNA was removed from nucleic acid preparations using DNA-free DNase (Ambion/Life Technologies) and purified using ethanol precipitation. The resulting preparations containing RNA were purified of ribosomal RNA using RiboZero (Illumina). Messenger RNA (mRNA) libraries were prepared for sequencing using a NEBNext Ultra Directional RNA Library Kit (New England Biolabs) with a modified protocol using Sera-Mag SpeedBeads that retain mRNA transcripts as small as 50 bp in length. The resulting mRNA libraries were verified using gel electrophoresis and a Bioanalyzer, multiplexed, and sequenced using an Illumina HiSeq 2500 (Illumina) in rapid mode.

The resulting sequence files were processed using the customized Python scripts align_barcode and filter_P7adapter (which was written by our laboratory), aligned using Bowtie 2 (ref. [31]), and analysed using the customized scripts tabulateFrequencies and annotateTabulated (written by our laboratory in Python and Perl). The representation of each mRNA transcript was determined by dividing the number of reads in a particular region by the total number of reads for the library.

**Fabrication of microfluidic devices.** Microfluidic devices were fabricated using standard soft lithography techniques. Devices were designed in AutoCAD (Autodesk) and masks were printed by CAD/Art Services. Device moulds were produced on silicon wafers (University Wafer) spin coated with SU-8 photoresist (MicroChem). Polydimethylsiloxane chips were plasma bonded to glass slides at least 24 h before use.

The devices used to conduct the RNA-Seq experiment had 12 parallel channels 400 μm wide × 100 μm high × 5 cm long. All 12 channels shared a single inlet port and a single outlet port. These chips were bonded to Corning 75 mm × 50 mm × 1 mm plain microslides.

The devices used to culture flow-shielded and flow-exposed subpopulations were described previously[26]. The channels were 50 μm high, 500 μm wide in the central channel and 50 μm wide in the crevices. The devices used to culture biofilm streamers were previously described[7]. The channels were 100 μm wide × 90 μm high. Each channel possessed its own inlet and outlet port. All of these chips were bonded to 36 mm × 60 mm number 1.5 coverglass (Ted Pella).

The devices used to measure *fro* expression at different shear rates had two parallel channels 500 μm wide × 50 μm high × 1 cm long. Each of the channels

possessed its own inlet and outlet port. The devices used to measure *fro* expression in different mutant backgrounds had 5 parallel channels 500 µm wide × 50 µm high × 2 cm long. Each of the channels possessed its own inlet and outlet port. These chips were bonded to Fisherbrand 22 mm × 60 mm number 1 coverglass.

***P. aeruginosa* growth in microfluidic devices.** In the experiments measuring *fro* expression, cells from mid-log phase cultures were injected directly into the flow chamber inlet with a pipette and allowed to settle for 10 min. The flow chamber was fixed on the microscope stage. A plastic, LB-filled, 27 G needle-tipped syringe mounted on a syringe pump (KD Scientific Legato 210) was connected to the chamber inlet via tubing (BD Intramedic Polyethylene Tubing; 0.38 mm inside diameter 1.09 mm outside diameter). The chamber outlet was connected to a waste container via tubing. The syringe pump was used to generate flow rates of 0.1–50 µl min$^{-1}$.

To coat the channel surfaces with MPTMS, we used a previously described method[20]. Briefly, channels were washed with a 5:1:1 $H_2O$:$H_2O_2$:HCl solution for 5 min, flushed with $H_2O$, treated with MPTMS for 30 min, and flushed with $H_2O$ again before adding cells.

For transcriptional profiling assays, cells from mid-log phase cultures were injected into the flow chamber inlet using a plastic syringe, and allowed to settle for 10 min. The flow chamber was fixed on the benchtop. A plastic, LB-filled, needle-tipped syringe mounted on a syringe pump was connected to the chamber inlet via tubing (McMaster-Carr Polyethylene Tubing 2 mm inside diameter, 4 mm outside diameter). The chamber outlet was connected to a waste container via tubing. The syringe pump was used to generate a flow rate of 100 µl min$^{-1}$.

**Shear rate and shear force calculations.** The shear rate at the floor and ceiling of the channel of the rectangular cross-section (where the height was less than the width) was calculated by the equation:

$$\text{shear rate} = \frac{6Q}{wh^2}$$

where $Q$ is the flow rate, $w$ is the channel's width and $h$ is the channel's height.

Shear stress was calculated as the product of shear rate and viscosity, as shown in Fig. 4c. Shear force was calculated as the product of shear stress and the surface area of a cell, which was estimated as 2.5 µm$^2$.

**Phase contrast and fluorescence microscopy.** Images were obtained with a Nikon Ti-E microscope controlled by NIS Elements (version 3.22.15). The microscope was equipped with a Nikon 10× Plan Fluor Ph1 0.3 NA objective, a Nikon 20× Plan Fluor Ph1 0.45 NA objective, a Nikon 40× Plan Apo Ph2 0.95 NA objective, a Nikon 60× Plan Apo 1.2 NA objective, × Plan Apo Ph3 1.4 NA objective, a Prior Lumen 200 Pro and an Andor Clara charge-coupled device camera.

**Quantification of *fro* expression.** The image analysis pipeline (Supplementary Fig. 1) was written in MATLAB (Mathworks). Cell masks were developed from phase contrast images using a Sobel operator edge-detection algorithm. The YFP and mCherry fluorescence intensities per masked cell were computed. The YFP-to-mCherry ratio of hundreds of individual cells was averaged and expressed as *fro* expression.

**Quantification of Ficoll viscosity.** To estimate the microscale viscosity of different Ficoll concentrations, we analysed the diffusion of optically trapped 500 nm polystyrene beads[32]. In brief, a 10 s time trace of the bead fluctuation $x(t)$ was recorded at a 50 kHz sampling rate. We then computed the positional autocorrelation $\mathrm{AC}(\tau) = \frac{1}{T}\int_0^T x(t+\tau)x(t)\mathrm{d}t \sim e^{-\frac{\tau}{\tau_c}}$, which yielded the autocorrelation time $\tau_c = \kappa/\gamma$, where $\kappa$ is the force sensitivity of the optical trap and depends on the laser power and size of the trapped bead only, and hence is constant. $\gamma = 3\pi D\eta$ is the viscous drag coefficient of the bead with diameter $D$ immersed in the Ficoll solution with viscosity $\eta$. We then compared the autocorrelation time of identical beads in water with those of different Ficoll concentrations to obtain the Ficoll viscosity $\eta_{\mathrm{Ficoll}}/\eta_{\mathrm{water}} = \tau_{\mathrm{water}}/\tau_{\mathrm{Ficoll}}$ relative to water.

**Reporting Summary.** Further information on research design is available in the Nature Research Reporting Summary linked to this article.

## Data availability

The data supporting the findings of the study are available in this article and its Supplementary Information files. All of the RNA-Seq data used to reach the conclusions of this paper are freely available under the National Center for Biotechnology Information Sequence Read Archive accession number PRJNA530209. Additionally, the raw data that support the findings of this study are available from the corresponding author upon request.

## Code availability

The custom MATLAB routines used for processing and analysing the fluorescence microscopy data are freely available from the corresponding author upon request. The custom Python and Perl scripts used for processing and analysing the RNA-Seq data are freely available from the corresponding author upon request.

Received: 14 October 2018; Accepted: 11 April 2019;
Published online: 13 May 2019

## References

1. Hansen, C. E., Qiu, Y., McCarty, O. J. T. & Lam, W. A. Platelet mechanotransduction. *Annu. Rev. Biomed. Eng.* **20**, 253–275 (2018).
2. Vollrath, M. A., Kwan, K. Y. & Corey, D. P. The micromachinery of mechanotransduction in hair cells. *Annu. Rev. Neurosci.* **30**, 339–365 (2007).
3. Persat, A. et al. The mechanical world of bacteria. *Cell* **5**, 988–997 (2015).
4. Hughes, K. T. & Berg, H. C. The bacterium has landed. *Science* **358**, 446–447 (2017).
5. Alsharif, G. et al. Host attachment and fluid shear are integrated into a mechanical signal regulating virulence in *Escherichia coli O157:H7*. *Proc. Natl Acad. Sci. USA* **17**, 5503–5508 (2015).
6. Rodesney, C. A. et al. Mechanosensing of shear by *Pseudomonas aeruginosa* leads to increased levels of the cyclic-di-GMP signal initiating biofilm development. *Proc. Natl Acad. Sci. USA* **23**, 5906–5911 (2017).
7. Drescher, K., Shen, Y., Bassler, B. L. & Stone, H. A. Biofilm streamers cause catastrophic disruption of flow with consequences for environmental and medical systems. *Proc. Natl Acad. Sci. USA* **11**, 4345–4350 (2013).
8. Sakariassen, K. S., Orning, L. & Turitto, V. T. The impact of blood shear rate on arterial thrombus formation. *Future Sci. OA* **4**, FSO30 (2015).
9. Gordon, A. et al. Single-cell quantification of molecules and rates using open-source microscope-based cytometry. *Nat. Methods* **2**, 175–181 (2007).
10. Boechat, A. L., Kaihami, G. H., Politi, M. J., Lepine, F. & Baldini, R. L. A novel role for an ECF sigma factor in fatty acid biosynthesis and membrane fluidity in *Pseudomonas aeruginosa*. *PLoS ONE* **12**, e84775 (2013).
11. Persat, A., Inclan, Y. F., Engel, J. N., Stone, H. A. & Gitai, Z. Type IV pili mechanochemically regulate virulence factors in *Pseudomonas aeruginosa*. *Proc. Natl Acad. Sci. USA* **24**, 7563–7568 (2015).
12. Lee, C. K. et al. Multigenerational memory and adaptive adhesion in early bacterial biofilm communities. *Proc. Natl Acad. Sci. USA* **17**, 4471–4476 (2018).
13. Inclan, Y. F. et al. A scaffold protein connects type IV pili with the Chp chemosensory system to mediate activation of virulence signaling in *Pseudomonas aeruginosa*. *Mol. Microbiol.* **4**, 590–605 (2016).
14. Luo, Y. et al. A hierarchical cascade of second messengers regulates *Pseudomonas aeruginosa* surface behaviors. *mBio* **1**, e02456-14 (2015).
15. Ellison, C. K. et al. Obstruction of pilus retraction stimulates bacterial surface sensing. *Science* **358**, 535–538 (2017).
16. Siryaporn, A., Kuchma, S. L., O'Toole, G. A. & Gitai, Z. Surface attachment induces *Pseudomonas aeruginosa* virulence. *Proc. Natl Acad. Sci. USA* **47**, 16860–16865 (2014).
17. Hug, I., Deshpande, S., Sprecher, K. S., Pfohl, T. & Jenal, U. Second messenger-mediated tactile response by a bacterial rotary motor. *Science* **358**, 531–534 (2017).
18. McCarter, L., Hilmen, M. & Silverman, M. Flagellar dynamometer controls swarmer cell differentiation of *V. parahaemolyticus*. *Cell* **3**, 345–351 (1988).
19. Brimer, C. D. & Montie, T. C. Cloning and comparison of *fliC* genes and identification of glycosylation in the flagellin of *Pseudomonas aeruginosa* a-type strains. *J. Bacteriol.* **12**, 3209–3217 (1998).
20. Siryaporn, A., Kim, M. K., Shen, Y., Stone, H. A. & Gitai, Z. Colonization, competition, and dispersal of pathogens in fluid flow networks. *Curr. Biol.* **9**, 1201–1207 (2015).
21. Chen, S. & Springer, T. A. Selectin receptor-ligand bonds: formation limited by shear rate and dissociation governed by the Bell model. *Proc. Natl Acad. Sci. USA* **3**, 950–955 (2001).
22. Martinez, V. A. et al. Flagellated bacterial motility in polymer solutions. *Proc. Natl Acad. Sci. USA* **50**, 17771–17776 (2014).
23. Potvin, E. et al. In vivo functional genomics of *Pseudomonas aeruginosa* for high-throughput screening of new virulence factors and antibacterial targets. *Environ. Microbiol.* **12**, 1294–1308 (2003).
24. Skurnik, D. et al. A comprehensive analysis of in vitro and in vivo genetic fitness of *Pseudomonas aeruginosa* using high-throughput sequencing of transposon libraries. *PLoS Pathog.* **9**, e1003582 (2013).
25. Cornforth, D. M. et al. *Pseudomonas aeruginosa* transcriptome during human infection. *Proc. Natl Acad. Sci. USA* **22**, E5125–E5134 (2018).
26. Kim, M. K., Ingremeau, F., Zhao, A., Bassler, B. L. & Stone, H. A. Local and global consequences of flow on bacterial quorum sensing. *Nat. Microbiol.* **1**, 15005 (2016).
27. Helmann, J. D. The extracytoplasmic function (ECF) sigma factors. *Adv. Microb. Physiol.* **46**, 47–110 (2002).
28. Lesic, B. & Rahme, L. G. Use of the lambda Red recombinase system to rapidly generate mutants in *Pseudomonas aeruginosa*. *BMC Mol. Biol.* **9**, 20 (2008).
29. Choi, K. H. & Schweizer, H. P. mini-Tn7 insertion in bacteria with single attTn7 sites: example *Pseudomonas aeruginosa*. *Nat. Protoc.* **1**, 153–161 (2006).

30. Hoang, T. T., Kutchma, A. J., Becher, A. & Schweizer, H. P. Integration-proficient plasmids for *Pseudomonas aeruginosa*: site-specific integration and use for engineering of reporter and expression strains. *Plasmid* **43**, 59–72 (2000).
31. Langmead, B. & Salzberg, S. L. Fast gapped-read alignment with Bowtie 2. *Nat. Methods* **9**, 357–359 (2012).
32. Koch, M. D. & Shaevitz, J. W. Introduction to optical tweezers. *Methods Mol. Biol.* **1486**, 3–24 (2017).

## Acknowledgements

We thank K. Kim for assistance with generating the flow-shielded and biofilm streamer microfluidic channels. We also thank members of the Gitai laboratory, J. Shaevitz, N. Wingreen, D. Kearns and L. Wiltbank for helpful discussions and comments on the manuscript. This work was supported by a grant (DP1AI124669) from the National Institutes of Health (to Z.G.). Additional funding came from the National Science Foundation (PHY-1734030 to B.P.B. and M.D.K.), Glenn for Aging Research (B.P.B.), DFG award KO5239/1-1 from the German Research Foundation (to M.D.K.), and National Institutes of Health grants K22AI112816 (to A.S.) and R21AI121828 (to B.P.B. and M.D.K.).

## Author contributions

J.E.S., A.L., M.D.K., A.S., H.A.S. and Z.G. designed the experiments. J.E.S., A.L., M.D.K. and A.S. performed the experiments. B.P.B. and A.S. conducted the computational analyses. J.E.S. and Z.G. wrote the paper.

## Competing interests

The authors declare no competing interests.

## Additional information

**Supplementary information** is available for this paper at https://doi.org/10.1038/s41564-019-0455-0.

**Reprints and permissions information** is available at www.nature.com/reprints.

**Correspondence and requests for materials** should be addressed to Z.G.

**Publisher's note:** Springer Nature remains neutral with regard to jurisdictional claims in published maps and institutional affiliations.

nature research

Corresponding author(s): Zemer Gitai

# Reporting Summary

Nature Research wishes to improve the reproducibility of the work that we publish. This form provides structure for consistency and transparency in reporting. For further information on Nature Research policies, see Authors & Referees and the Editorial Policy Checklist.

## Statistical parameters

When statistical analyses are reported, confirm that the following items are present in the relevant location (e.g. figure legend, table legend, main text, or Methods section).

| n/a | Confirmed | |
|---|---|---|
| ☐ | ☒ | The exact sample size (*n*) for each experimental group/condition, given as a discrete number and unit of measurement |
| ☐ | ☒ | An indication of whether measurements were taken from distinct samples or whether the same sample was measured repeatedly |
| ☐ | ☒ | The statistical test(s) used AND whether they are one- or two-sided<br>*Only common tests should be described solely by name; describe more complex techniques in the Methods section.* |
| ☒ | ☐ | A description of all covariates tested |
| ☒ | ☐ | A description of any assumptions or corrections, such as tests of normality and adjustment for multiple comparisons |
| ☒ | ☐ | A full description of the statistics including central tendency (e.g. means) or other basic estimates (e.g. regression coefficient) AND variation (e.g. standard deviation) or associated estimates of uncertainty (e.g. confidence intervals) |
| ☒ | ☐ | For null hypothesis testing, the test statistic (e.g. *F*, *t*, *r*) with confidence intervals, effect sizes, degrees of freedom and *P* value noted<br>*Give P values as exact values whenever suitable.* |
| ☒ | ☐ | For Bayesian analysis, information on the choice of priors and Markov chain Monte Carlo settings |
| ☒ | ☐ | For hierarchical and complex designs, identification of the appropriate level for tests and full reporting of outcomes |
| ☒ | ☐ | Estimates of effect sizes (e.g. Cohen's *d*, Pearson's *r*), indicating how they were calculated |
| ☐ | ☒ | Clearly defined error bars<br>*State explicitly what error bars represent (e.g. SD, SE, CI)* |

*Our web collection on statistics for biologists may be useful.*

## Software and code

Policy information about availability of computer code

| | |
|---|---|
| Data collection | We used NIS Elements (version 3.22.15) to collect imaging data. |
| Data analysis | We used custom MATLAB (R2018a) code to quantify fluorescence intensity. We also used custom Python code to analyze RNA-sequencing data. We also used BowTie 2 and custom Perl scripts to analyze RNA-sequencing data. The code will be available upon request after publication. |

For manuscripts utilizing custom algorithms or software that are central to the research but not yet described in published literature, software must be made available to editors/reviewers upon request. We strongly encourage code deposition in a community repository (e.g. GitHub). See the Nature Research guidelines for submitting code & software for further information.

## Data

Policy information about availability of data

All manuscripts must include a data availability statement. This statement should provide the following information, where applicable:

- Accession codes, unique identifiers, or web links for publicly available datasets
- A list of figures that have associated raw data
- A description of any restrictions on data availability

Figure 1 and supplemental tables S1 and S2 have associated raw sequencing data. Most of the figures have associated raw images. All of this raw data will be available upon request after publication.

# Field-specific reporting

Please select the best fit for your research. If you are not sure, read the appropriate sections before making your selection.

☒ Life sciences ☐ Behavioural & social sciences ☐ Ecological, evolutionary & environmental sciences

For a reference copy of the document with all sections, see nature.com/authors/policies/ReportingSummary-flat.pdf

# Life sciences study design

All studies must disclose on these points even when the disclosure is negative.

| | |
|---|---|
| Sample size | For quantification of individual cells, we measured 30 or more cells. We considered a given experiment that included at least 30 cells to be one experimental replicate, and calculated the standard deviation of data from at least three experiments. This sample size was sufficient to support our conclusions as it led to standard deviations across replicates that were much smaller than the experimental effects from which were drawing conclusions. |
| Data exclusions | No data was excluded. |
| Replication | All quantified experiments were performed independently at least three times. There were no experiments that could not be replicated or reproduced. |
| Randomization | Randomization was not relevant to this study, as all experiments are performed on bacterial strains grown in broth culture, which were then split in different treatment conditions. |
| Blinding | No blinding was used. Blinding was not relevant to this study, as we used the same set of data acquisition and analysis parameters for each biological sample. |

# Reporting for specific materials, systems and methods

### Materials & experimental systems

| n/a | Involved in the study |
|---|---|
| ☐ | ☒ Unique biological materials |
| ☒ | ☐ Antibodies |
| ☒ | ☐ Eukaryotic cell lines |
| ☒ | ☐ Palaeontology |
| ☒ | ☐ Animals and other organisms |
| ☒ | ☐ Human research participants |

### Methods

| n/a | Involved in the study |
|---|---|
| ☒ | ☐ ChIP-seq |
| ☒ | ☐ Flow cytometry |
| ☒ | ☐ MRI-based neuroimaging |

## Unique biological materials

Policy information about availability of materials

| | |
|---|---|
| Obtaining unique materials | All strains and plasmids will be available upon request after publication. |